Progress In Electromagnetics Research M, Vol. 106, 167–177, 2021

A Novel Miniaturized C-Band Bandpass Filter

Luyao Tang, Xiaoli Jiang, Hao Wei, and Weiwei Liu*

Abstract—A novel miniaturized bandpass filter (BPF) is proposed, which is based on a stepped-impedance resonator (SIR) and cross-coupling theory. This filter has the characteristics of small size and high out-of-band rejection. The filter consists of four 1/2 wavelength stepped-impedance resonators and two 1/4 wavelength short-circuit microstrip resonators. By designing a new kind of structure, the cross coupling is realized between the second and fifth resonators, and two transmission zeros are introduced out of band. Zero-degree feeding is realized due to the symmetry of the structure and feeding position, which adds two other transmission zeros outside the band. Four transmission zeros are introduced outside the passband of the filter, which greatly increase the out-of-band rejection of the filter. The passband of the filter is 3.2 GHz–4.2 GHz, and the out-of-band rejection at 2.6 GHz and 4.8 GHz reaches −60 dB. The size of the filter is only 7.2 mm ∗ 8 mm ($0.21\lambda_g * 0.24\lambda_g$), which realizes the miniaturization of the filter.

1. INTRODUCTION

As a frequency selective device for separating signals from different frequencies, filters are widely used in various communication systems such as satellite communication [1], Wi-Fi [2], ship electronics [3], and communication base stations [4]. In recent years, the demand for filters in communication systems is developing towards miniaturization, low cost, and high performance [5–7]. The filter is miniaturized mainly from three aspects: (1) miniaturized resonator, (2) compact structure, (3) new materials or processes. Miniaturized resonators are the basis of realizing the miniaturization of filters, such as capacitor loaded resonators and step impedance resonators (SIR) [8–10], all of which can achieve smaller size than traditional resonators. SIR was first proposed by Japanese scholars in 1980. It has the advantages of miniaturization and controllable parasitic passband, and has been widely used [9]. In [10], a novel bandpass filter by loading a SIR is presented, which reduces the size by 38% compared with the conventional hairpin-line filter with the same technical specifications. Although the filter size in the reference is smaller than that in the traditional filter structure, there is still the possibility of improvement in size and suppression. Due to the flexible and adjustable high-order harmonics of SIR, in recent years, researchers often use its multimode resonance to design UWB filters or multi passband filters. However, these filters generally do not have enough out of band suppression [11, 12]. Besides, hairpin structure, folded structure, and defective ground structure are also critical for designing compact and miniaturized filters. With the development and maturity of new materials and processes such as thin film process [13], low-temperature co-fired ceramics (LTCC) [14], and micro-electromechanical systems (MEMS) [15], they provide more flexible design methods for the miniaturization of filters. However, both LTCC and MEMS have higher production costs and lower yields.

In this paper, a compact bandpass filter is designed with a Cascaded Quadruplet (CQ) topology composed of four folded SIRs and two short-circuit resonators, which achieves miniaturization and high

Received 21 September 2021, Accepted 7 December 2021, Scheduled 24 December 2021
* Corresponding author: Weiwei Liu (1715914830@qq.com).
The authors are with The 54th Research Institute of China Electronics Technology Group Corporation (CETC-54), Shijiazhuang 050051, China.

out-of-band rejection. CQ topology successfully achieves two finite transmission zeros (TZs) in the upper and lower sidebands of the filter by proper electric coupling and magnetic coupling. The coupling matrix of the filter is obtained through the filter synthesis theory. The related curve between the coupling coefficient and the distance of each resonator is obtained by the HFSS software simulation. Combining symmetrical structure and feeding position, a miniaturized filter with four transmission zeros and high out-of-band rejection is successfully realized. Finally, the filter is processed on a 0.254 mm-thickness Alumina ceramic substrate which has a loss tangent $\tan\delta$ of 0.002 and relative dielectric constant ε_r of 9.8 by thin film technology. The measured results of the filter are very similar to the simulation ones. Compared with other filters, this filter has smaller size and higher out-of-band rejection.

2. DESIGN OF 6-ORDER CROSS-COUPLED BANDPASS FILTER

The technical specifications of the filter to be designed are as follows. Passband frequency range: 3.2 GHz–4.2 GHz (Fractional bandwidth: 27%); In-band flatness: 1 dB; In-band insertion loss: 2 dB; In-band standing-wave ratio: 1.5; Out-of-band rejection: 30 dB @ 2.8 GHz & 4.6 GHz; 40 dB @ 2.6 GHz & 4.8 GHz.

2.1. Filter Topology and Coupling Matrix

It is obvious that the key problem to design the filter is the conflict of the wide bandwidth and high rejection. Comparing the characteristics of Chebyshev, Butterworth and elliptic function filter models, Chebyshev model is chosen to design the filter. According to Chebyshev model, the filter order is calculated as follows:

$$n > \left\lceil \frac{ch^{-1}\sqrt{\dfrac{10^{\frac{L_{As}}{10}}}{\varepsilon}}}{ch^{-1}\Omega_S} \right\rceil \tag{1}$$

where n is the order of the filter, L_{AS} the out-of-band rejection, ε the ripple factor, and Ω_S the stopband frequency. Combining in-band flatness and standing-wave ratio, the ripple factor ε is selected as 0.01. In this case, $n > 7.13$. The filter designed by Chebyshev model needs at least eight orders to meet the high out-of-band rejection. This is disadvantageous to the miniaturization of the filter. The generalized Chebyshev function model is considered to design the filter. Generalized Chebyshev function model has the same in-band and edge characteristics as traditional Chebyshev model [16]. Compared with Chebyshev model, which can only generate transmission zero at infinity, generalized Chebyshev model can generate transmission zero at finite frequency, and transmission zero does not require symmetry about passband. This can greatly increase the out-of-band rejection of the filter and realize the high-performance filter with fewer resonators. Considering the specific design index of the filter, the sixth-order generalized Chebyshev model is proposed to design the filter.

It is necessary to determine the appropriate filter topology before synthesizing the coupling matrix of the filter. For a six-order filter, if Cascade Triangle (CT) topology is used to generate two transmission zeros, all six resonators need to participate in cross coupling [16]. This increases the difficulty of structural design. This paper adopts the topological structure shown in Fig. 1. Resonators 2, 3, 4, and 5 form a CQ topology, and resonators 1 and 6 are coupled with the feeding point and CQ structure to form the whole filter structure, but resonators 1 and 6 do not participate in cross coupling. The principle that the CQ structure can generate transmission zeros is analyzed below.

To achieve a wide bandwidth of 27%, it is necessary to introduce enough coupling strength which can be achieved by increasing the coupling length as long as possible. For microstrip coupling, when the coupling length is greater than $1/4 * \lambda_g$, the magnetic coupling is the main coupling which is realized by inductance [17]. The signal will undergo a -90° phase shift when being transmitted by magnetic coupling. In the resonator, when the resonant frequency is greater than the transmission frequency, the signal will have a phase shift of $+90^\circ$. On the contrary, when the resonance is less than the transmission

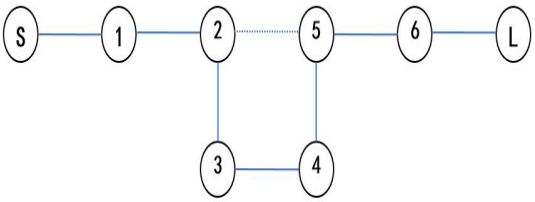

Figure 1. Topological structure of sixth-order cross-coupled filter.

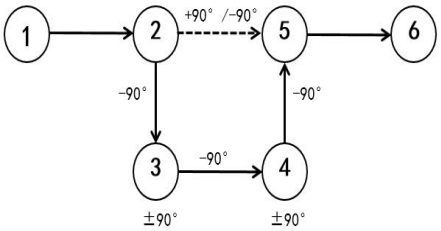

Figure 2. Cross-coupled CQ topology.

frequency, the signal will have a phase shift of $-90°$ [16]. The CQ topology of filter cross-coupling and the corresponding signal phase shift is shown in Fig. 2. Resonator 2 and resonator 5 can be realized by electric coupling or magnetic coupling, and their specific phase shift effects on signals are shown in Table 1. It can be concluded from the analysis in the table that only when resonator 2 and resonator 5 are electrically coupled, the CQ topology can generate a transmission zero in the upper and lower stopbands of the filter passband. The position of the transmission zero point is determined by the coupling strength of resonator 2 and resonator 5.

Table 1. CQ topological phase change of electric/magnetic cross coupling.

	transmission route	$f > f_0$ phase shift	$f > f_0$ phase shift
Electric cross coupling ($+90°$)	$2 \to 3 \to 4 \to 5$	$-90° - 90° - 90° - 90°$ $-90° = -450°$	$-90° + 90° - 90° + 90°$ $-90° = -90°$
	$2 \to 5$	$+90°$	$+90°$
Magnetic cross coupling ($-90°$)	$2 \to 3 \to 4 \to 5$	$-90° - 90° - 90°$ $-90° - 90° = -450°$	$-90° + 90° - 90°$ $+90° - 90° = -90°$
	$2 \to 5$	$-90°$	$-90°$

After the order and topology of the filter are determined, the coupling matrix is extracted by combining the technical indexes of the filter (centre frequency 3.7 GHz, fractional bandwidth 27%). It is proposed to introduce two transmission zeros through cross coupling at 2.7 GHz and 4.6 GHz. Using the synthesis theory of cross-coupled filter [18–22], the coupling matrix M and external Q value of the sixth-order cross-coupled filter are obtained.

$$M = \begin{bmatrix} 0 & 0.2282 & 0 & 0 & 0 & 0 \\ 0.2282 & 0 & 0.1624 & 0 & -0.0186 & 0 \\ 0 & 0.1624 & 0 & 0.1720 & 0 & 0 \\ 0 & 0 & 0.1720 & 0 & 0.1639 & 0 \\ 0 & -0.0186 & 0 & 0.1639 & 0 & 0.2283 \\ 0 & 0 & 0 & 0 & 0.2283 & 0 \end{bmatrix}$$

The external Q value $Q_{es} = Q_{el} = 3.68$.

2.2. Derivation of Physical Size of Filter

The filter is cross-coupled by CQ structure composed of four SIRs, and the whole filter structure is formed by coupling with two other $1/4 * \lambda_g$ short-circuit resonators. The basic structure of SIR is shown

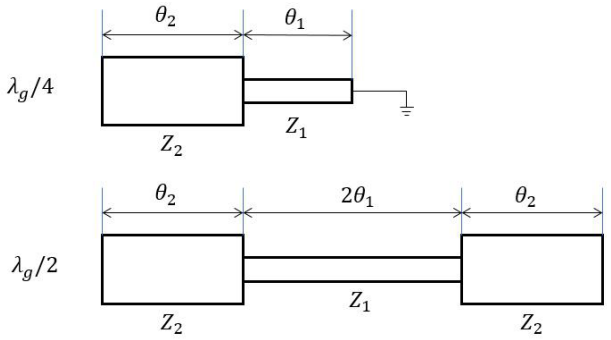

Figure 3. Basic structure of SIR.

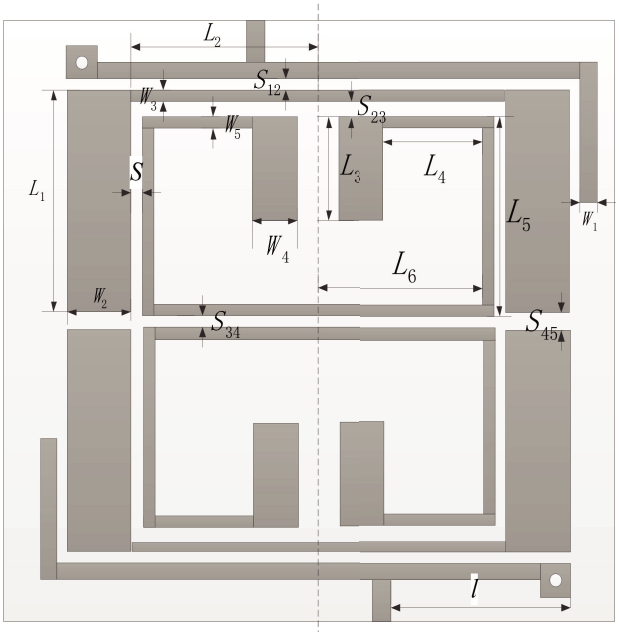

Figure 4. Structure of the proposed miniaturized BPF.

in Fig. 3. The resonance condition can be expressed as:

$$R_Z = \frac{Z_2}{Z_1} = \tan\theta_1 \tan\theta_2 \tag{2}$$

where R_Z is the impedance ratio. It is defined as $R_Z = \frac{Z_2}{Z_1}$. When the selected impedance ratio is less than 1, the size of the SIR can be smaller than that of the uniform impedance resonator, which is beneficial to the miniaturization design of the filter.

The filter uses an alumina ceramic substrate with a relative dielectric constant of 9.8, loss tangent of 0.002, and thickness of 0.254 mm. The bottom layer of the substrate is the ground of the filter, and the top layer is the microstrip line with a special shape and different impedances. The filter is processed by thin film processing technology. Under the thin film process, the minimum line width and line distance of the microstrip can reach 0.01 mm, which is beneficial to the design of wide-band filters requiring strong coupling. The novel structure of the filter is shown in Fig. 4. For the convenience of structural design, the impedance ratio R_Z of resonator 2 is assigned to 0.33, and then $Z_1 = 71.48\,\Omega$ and $Z_2 = 23.59\,\Omega$ are selected. The impedance ratio R_Z of resonator 3 is assigned to 0.5, and then $Z_1 = 61.56\,\Omega$ and $Z_2 = 30.78\,\Omega$ are selected. Based on the resonance condition of formula (2) and the center frequency of 3.7 GHz, the dimensions of two resonators are derived as follows: $W_2 = 0.85$ mm, $W_3 = 0.1$ mm, $W_4 = 0.58$ mm, $W_5 = 0.15$ mm, $L_1 = 2.56$ mm, $L_2 = 2.45$ mm, $L_3 = 1.24$ mm, $L_4 = 1.29$ mm, $L_5 = 2.4$ mm, $L_6 = 2.15$ mm, $S = 0.06$ mm. Resonator 1 and resonator 6 are short-circuit microstrip lines with a length of 8.02 mm and a width of 0.2 mm, which are coupled with the SIRs. For the same resonant frequency, the length of the short line with a via-hole is half of the open line length without a via-hole, which is conducive to the miniaturization of the filter.

After determining the size and shape of each resonator, the coupling distance between each resonator and the feeding position should be calculated so that the design of the whole filter can be completed. To calculate the coupling distance, the common method is to extract the related curve between the coupling coefficient and the distance between two resonators by means of the intrinsic simulation of HFSS software, and then calculate the coupling distance by combining the synthesized coupling matrix. The calculation formula of coupling coefficient is as follows:

$$\mathrm{k} = \frac{f_1^2 - f_2^2}{f_1^2 + f_2^2} \tag{3}$$

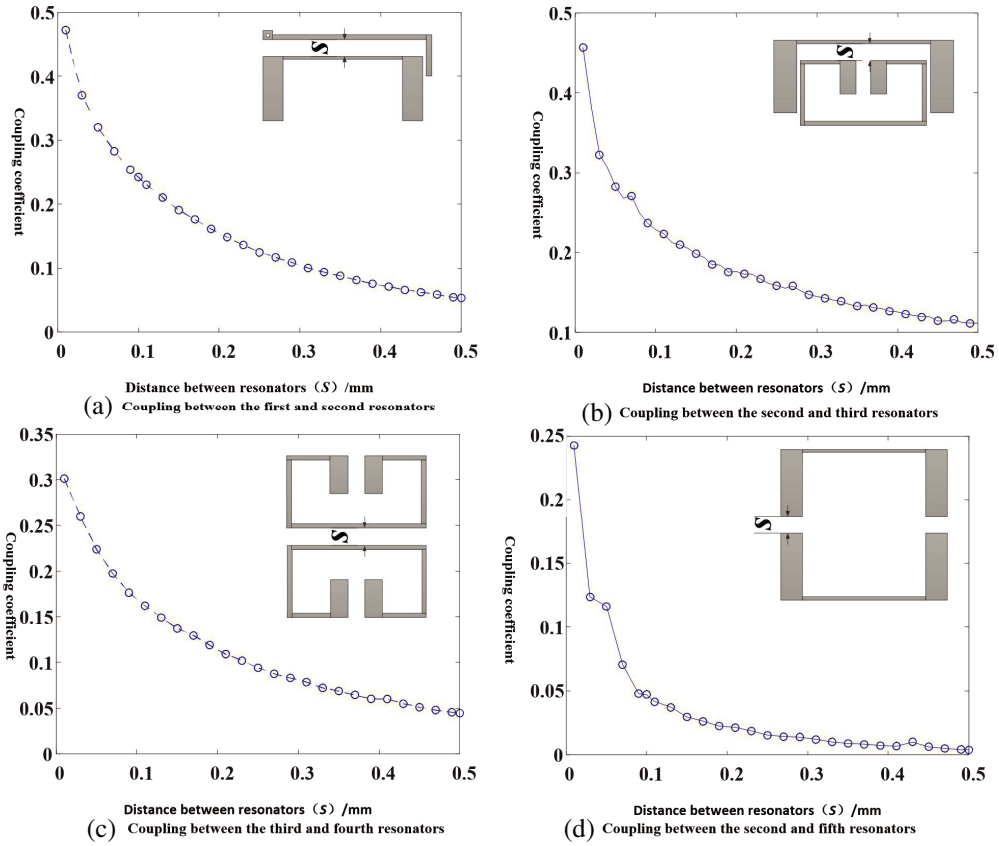

Figure 5. Curve of coupling coefficient changing with coupling distance.

where f_1 and f_2 are the first and second eigenmode frequencies of the coupled resonator. Besides that, f_1 and f_2 meet the formula $f_0 = \sqrt{f_1 * f_2}$, where f_0 is the centre frequency of the filter. Taking the coupling distance between the resonators as a variable, the scanning parameter simulation is carried out. The related curve between the coupling coefficient and the spacing of each resonator is shown in Fig. 5.

Combining the coupling matrix with the curve of coupling coefficient and distance in Fig. 5, we get $S_{12} = 0.13\,\text{mm}$, $S_{23} = 0.23\,\text{mm}$, $S_{34} = 0.11\,\text{mm}$, $S_{25} = 0.23\,\text{mm}$. Because of the cross coupling between resonator 2 and resonator 5, the energy coupled from resonator 2 to resonator 3 becomes less. It is necessary to fine-tune S_{23} and finally get $S_{23} = 0.21\,\text{mm}$.

The position of the input and output of the filter affects its external quality factor [23]. In order to determine the relationship between the required external quality factor and the feeding position, full-wave simulation analysis is carried out by using HFSS software. The relationship between the group delay of S_{11} and external quality factor Q_e is as follows.

$$\tau_{S_{11}}(f_0) = \frac{2Q_e}{\pi f_0} \tag{4}$$

Substituting external quality factor and center frequency, we get $\tau_{S_{11}}(f_0) = 630\,\text{ns}$. Taking the the feeding position l as a variable, the group delay is simulated, and the values of the group delay at different l values are obtained. The simulation results are shown in Fig. 6.

According to the above figure, when $l = 2.35\,\text{mm}$, the group delay of centre frequency meets the design value. At this point, all the structural parameters of the filter have been determined. The simulation results by HFSS software are shown in Fig. 7.

It can be seen from Fig. 7 that the passband of the filter is 3.2 GHz–4.2 GHz, and the in-band flatness is 0.3 dB. The out-of-band rejection at 2.6 GHz is −70 dB, and the out-of-band rejection at

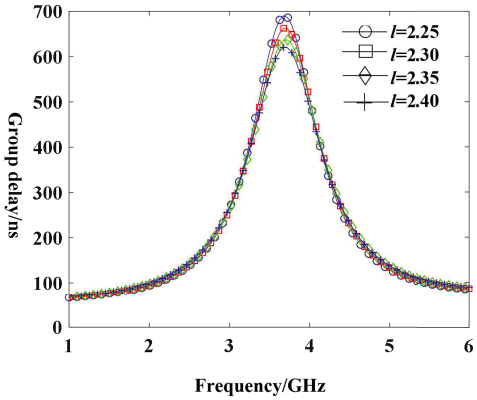

Figure 6. Group delay curves under different variables l.

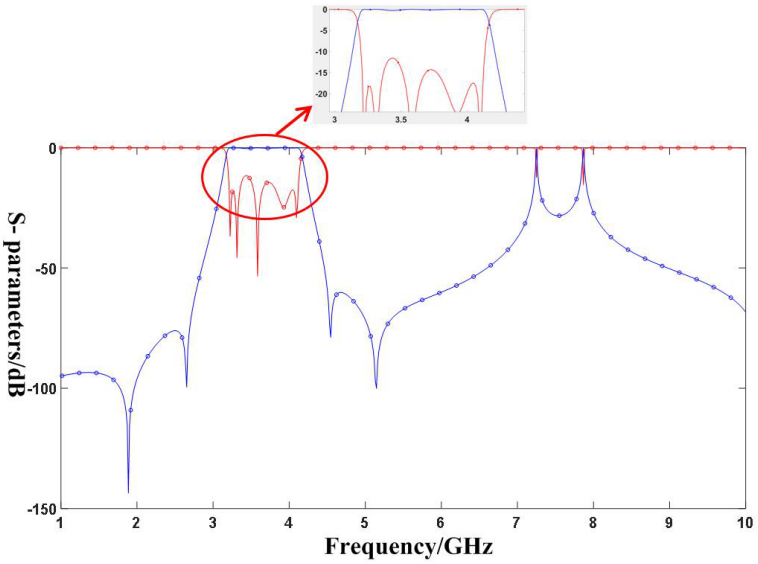

Figure 7. S parameters of filter simulation.

4.8 GHz is −60 dB, which is much higher than the index requirement of −40 dB. The designed filter generates four transmission zeros, two of which are generated by cross coupling structure, and the other two are generated by zero-degree feeding structure. The generation of transmission zeros is explained structurally below.

The CQ topology is cross coupled to generate transmission zeros at 2.68 GHz and 4.58 GHz. Electromagnetic coupling of CQ topology is shown in Fig. 8. The serial numbers 1, 2, 3, 4, 5, and 6 represent resonators. Resonators 2, 3, 4, and 5 form a cross coupling structure. Resonators 2 and 3, 3 and 4, 4 and 5 are coupled through long lines, mainly magnetic coupling. Resonators 2 and 5 are capacitively coupled through microstrip lines, mainly electrical coupling. Combined with the analysis of the influence of electromagnetic coupling on signal phase shift in Table 1, two transmission zeros will be formed in the upper and lower stopbands of the filter. The position of the transmission zeros is determined by the coupling strength between resonators 2 and 5, that is, the spacing between resonators 2 and 5. In the paper, the coupling matrix is synthesized under the condition of introducing transmission zeros at 2.7 GHz and 4.6 GHz, and the coupling coefficients are obtained. The structure size of cross coupling can be determined by the relationship curve between coupling coefficient and coupling spacing in Fig. 5. The simulation results show that the transmission zeros are 2.68 GHz and 4.58 GHz, which are very close to the theoretical value.

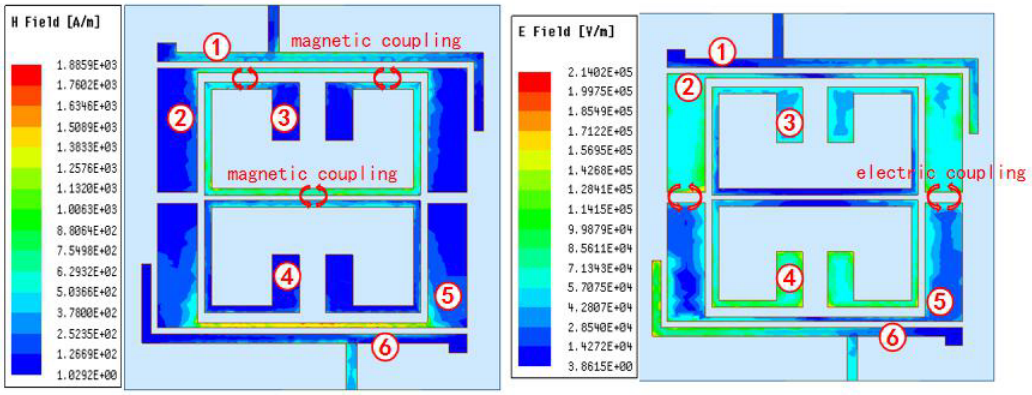

Figure 8. Coupled electromagnetic field of filter.

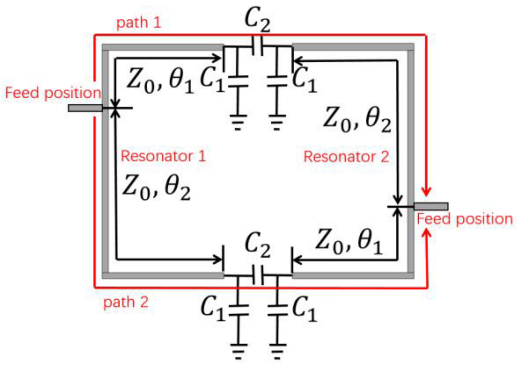

Figure 9. Typical zero-degree feeding structure.

The zero-degree feeding structure is the cause of the other two zeros. Fig. 9 shows a typical structure of zero-degree feeding. In the symmetrical structure, the phase shift difference between path 1 and path 2 is 0 degrees. Through the microwave network analysis, the transmission zero will be generated when $\theta_1 = \pi/2$ or $\theta_2 = \pi/2$. Similar symmetrical structures can also generate transmission zeros [24, 25]. The symmetrical structure and feeding position of the filter designed in this paper meet the zero-degree feeding condition, so two transmission zeros are generated at 1.67 GHz and 5.14 GHz. It improves the out-of-band rejection of the filter additionally.

Due to the existence of multimode resonant frequency of microstrip resonator, there is a spurious passband in the upper stopband of the filter, and its frequency range is 7.12 GHz to 7.9 GHz. With the help of eigenmode simulation of HFSS software. The secondary resonant frequency of each resonator is extracted. The secondary resonant frequencies of resonators 1, 2, and 3 are 10.75 GHz, 11.18 GHz, and 7.56 GHz respectively. The coupling of the second harmonic of each resonator forms the first spurious passband of the filter from 7.12 GHz to 7.9 GHz. Although there is a spurious passband, the out of band suppression of the filter below 6.75 GHz is greater than −40 dB.

2.3. Measurement and Analysis

In order to assure the accuracy of the designed values, thin film process is used to manufacture the filter. The physical diagram of the filter is shown in Fig. 10, and the size of the filter is 7.2 mm ∗ 8 mm. The filter is tested with Anritsu 3680 V test fixture and vector network analyzer.

The simulated and measured results of filter are shown in Fig. 11. As shown in Fig. 11, the simulation results are very conformable with the test results. The measured curve shows that the passband of the filter is 3.2 GHz–4.15 GHz. The insertion loss of the centre frequency is 2 dB, and the

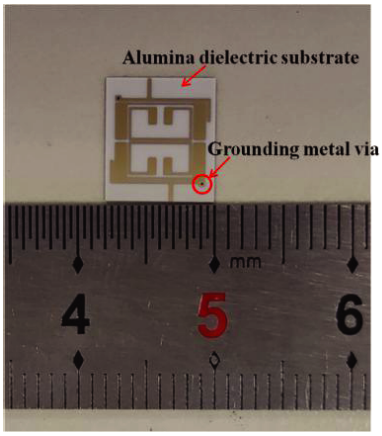

Figure 10. Photograph of the proposed bandpass filter.

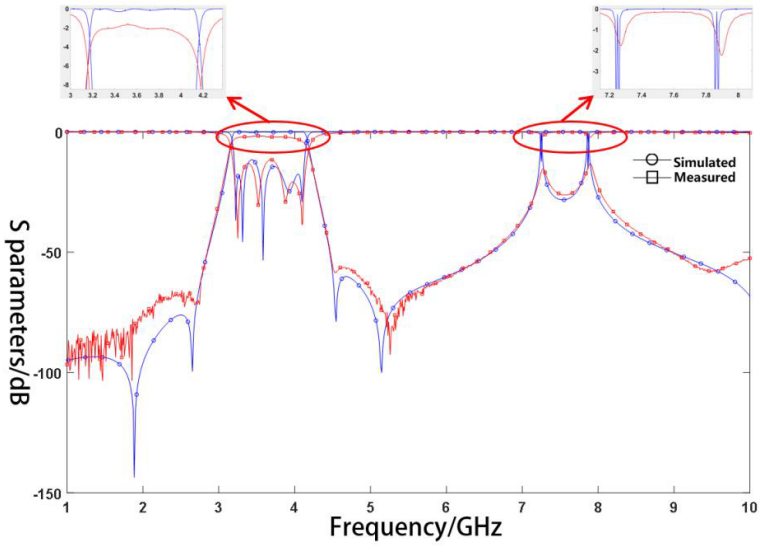

Figure 11. Comparison between simulated and measured results of filter.

standing wave ratio is 1.5. Out of band, the filter realized four transmission zeros as in the simulation results. The measured out-of-band rejections at 2.6 GHz and 4.8 GHz are −68 dB and −60 dB. Although there is a slight difference between the measured and the simulation results, due to the processing error which leads to the increase of the distance between resonators.

Considering that the filter will be micro-assembled in a conductor with other RF chips, we test the filter separately in the conductor box again, which is closer to the actual use. Fig. 12 shows the filter micro-assembled in the conductor box. During the test, a metal cover plate is covered on the top of the box. The measured results of the filter assembled in the conductor box are shown in Fig. 13. The measured out-of-band rejections at 2.6 GHz and 4.8 GHz are −62 dB and −55 dB. Comparing the two measured results, the filter shows less out of band attenuation when it is enclosed in a conductive box.

Compared with the previous works [26–30], the BPF designed in this paper has excellent out-of-band rejection with small size. There is main parameters comparison in Table 2. It can be seen from the table that the fractional bandwidth of the filter in this paper is wider than other filters, but its size is generally smaller than that of the filters in the literature. Especially for a wide fractional bandwidth of 27%, more resonators are needed theoretically. This makes it more difficult to miniaturize the filter. The paper further illustrates the superiority of the filter in miniaturization.

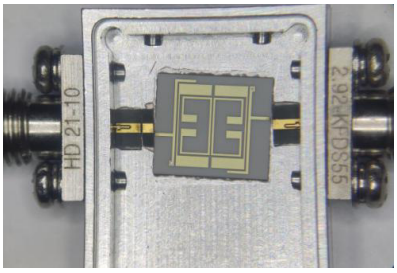

Figure 12. Micro assembled filter in conductor box.

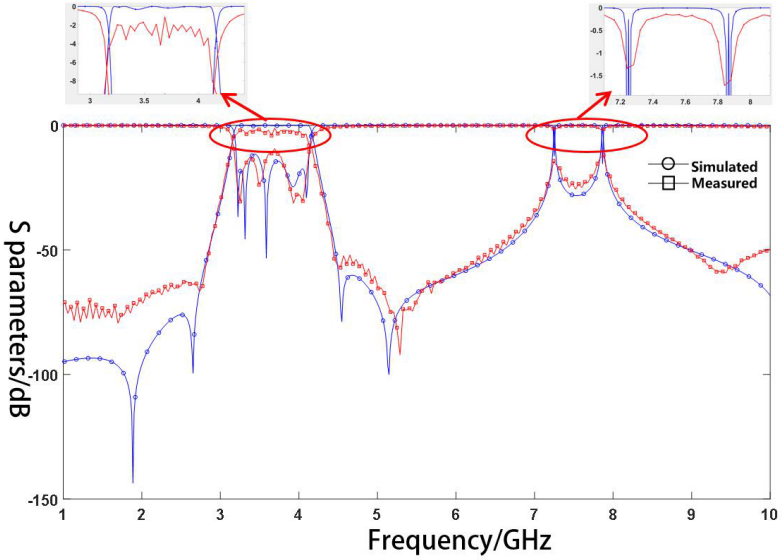

Figure 13. Comparison between simulated and measured results in conductor box.

Table 2. Comparison of various BPF.

Reference	f_0/GHz	FBW	TZs	Out-of-band Rejection (dB)	Size
[6]	2.4	15%	2	−30	$0.37\lambda_g * 0.26\lambda_g$
[10]	3.5	5.7%	4	−40	$0.4\lambda_g * 0.35\lambda_g$
[26]	8.6	9.3%	1	−55	$0.75\lambda_g * 0.68\lambda_g$
[27]	40.25	16.2%	0	−30	$0.52\lambda_g * 0.22\lambda_g$
[28]	2.0	15%	2	−20	$0.35\lambda_g * 0.4\lambda_g$
[29]	10.2	18.2%	2	−50	$0.79\lambda_g * 1.33\lambda_g$
[30]	1.3	85%	0	−20	$0.79\lambda_g * 1.33\lambda_g$
This Work	3.7	27%	4	−60	$0.45\lambda_g * 0.8\lambda_g$

3. CONCLUSION

A novel miniaturized bandpass filter with high out-of-band rejection is proposed. Transmission zeros are introduced through cross coupling of SIRs, and the technical specifications are achieved with fewer orders than traditional Chebyshev filters. With the help of HFSS software, the structure size and feed point position of the filter are derived. Because the symmetrical design of the filter structure and the

feeding position meet the zero-degree feeding condition, two extra transmission zeros are introduced outside the band, which greatly increases the out-of-band rejection of the filter. It is found that the measured results are very conformable with the simulation results. Compared with the bandpass filters of the same type in recent years, the filter in this paper has wider bandwidth, smaller size, and higher out-of-band rejection. The final size of the filter is only 7.2 mm $*$ 8 mm ($0.21\lambda_g * 0.24\lambda_g$), which realizes the miniaturization design of the filter.

REFERENCES

1. Wang, Q., H. Zheng, and J. Zhou, "A Ka satellite communication filter with high out-of-band rejection," *Acta Sinica Microwave*, Vol. S2, 344–347, 2016.
2. Aiswarya, S., S. Bhuvana Nair, L. Meenu, and S. K. Menon, "Analysis and design of stub loaded closed loop microstrip line filter for Wi-Fi applications," *2019 Sixteenth International Conference on Wireless and Optical Communication Networks (WOCN)*, 1–5, 2019.
3. Zhou, P., "Design and implementation of bandpass filter for shipborne solid-state navigation radar," *Automation and Instrumentation*, Vol. 31, No. 06, 69–73, 2016.
4. Solution, "5G application of ceramic dielectric filter," *Computer Products and Circulation*, No. 03, 88, 2020.
5. Wang, X., K. Yang, and Q. Li, "Miniaturization design of hairpin filter in Ku band," *Radio Communication Technology*, Vol. 44, No. 4, 420–424, 2018.
6. Ma, R., J. Yan, X. Chen, et al., "Design of a new miniaturized cross-coupled bandpass filter," *Chinese Journal of Testing Technology*, Vol. 30, No. 01, 69–73, 2016.
7. Tan, X., B. Jin, Z. Qian, et al., "Research on miniaturization technology of microwave filter," *Ship Electronic Countermeasure*, Vol. 36, No. 01, 83–87, 2013.
8. Xiao, D. and Q. He, "Design of comb cavity filter based on HFSS capacitor loading," *Communication World*, Vol. 27, No. 04, 129–130, 2020.
9. Makimoto, M. and S. Yamashita, *Microwave Resonators and Filters in Wireless Communication*, National Defense Industry Press, Beijing, 2002.
10. Zhang, M., M. Li, P.-J. Zhang, K. Duan, B. Jin, L. Huang, and Y. Song, "A novel minniaturized bandpass filter basing on stepped-impedance resonator," *Progress In Electromagnetics Research Letter*, Vol. 97, 77–85, 2021.
11. Żukociński, M., "A 5.8–10.6 GHz UWB filter using novel SIR structure," *2018 22nd International Microwave and Radar Conference (MIKON)*, 477–480, 2018.
12. Huang, L., P. Zhang, M. Li, Y. Song, and K. Duan, "Compact dual-wideband bandpass filter using stub loaded zero-degree feed coupling structure," *2019 Photonics & Electromagnetics Research Symposium — Fall (PIERS — Fall)*, 2169–2172, Xiamen, China, Dec. 17–20, 2019.
13. Zhao, C., K. Kisslinger, X. Huang, et al., "Bi-continuous pattern formation in thin films via solid-state interfacial dealloying studied by multimodal characterization," *Materials Horizons*, Vol. 6, No. 10, 1991–2002, 2019.
14. Liu, Y. and Y. Dai, "Research on miniaturization of LTCC band-pass filter loaded with capacitance," *Microcomputer and Applications*, Vol. 35, No. 10, 22–23+27, 2016.
15. Tang, X., Z. Jin, X. He, et al., "Optimal design of interdigital MEMS filter," *Piezoelectric and Acousto-optic*, Vol. 41, No. 04, 473–475+480, 2019.
16. Yu, K., "Extraction of coupling parameters of microwave filter," Xidian University, 2018.
17. Xiao, O., "Research on hybrid electromagnetic coupling filter," South China University of Technology, 2012.
18. Cameron, R. J., "Advanced coupling matrix synthesis techniques for microwave filters," *IEEE Transactions on Microwave Theory and Techniques*, Vol. 51, No. 01, 1–10, 2003.
19. Liu, J., "Finite transmission zero extraction and cross-coupling structure analysis of generalized Chebyshev filter," *Ship Electronic Engineering*, Vol. 35, No. 09, 59–62+118, 2015.

20. Bao, L., Z. Tang, and B. Zhang, "Design and research of a new CQ microstrip cross-coupling filter," *Semiconductor Technology*, Vol. 36, No. 01, 63–66+75, 2011.
21. Xiao, F., "Research on direct synthesis method of generalized Chebyshev bandpass filter," *Space Electronics Technology*, Vol. 9, No. 04, 90–93, 2012.
22. Qi, N., R. Zhang, and S. Li, "Direct synthesis method of microwave bandpass filters," *Space Electronics Technology*, Vol. 14, No. 04, 7–10+21, 2017.
23. Hong, J. S., *Microstrip Filters for RF/microwave Applications*, John Wiley&Sons, USA, 2004.
24. Chen, J., Y.-J. She, H.-H. Wang, Y. Liu, and N. Wang, "Design of compact tri-band filter based on SIR-loaded resonator with 0° feed," *2014 IEEE International Conference on Communiction Problem-solving*, 322–325, 2014.
25. Xia, Z. and F. Liu, "Dual-band bandpass filters using SIRs with open-stub line and zero-degree feed structure," *2013 IEEE International Wireless Symposium (IWS)*, 1–4, 2013.
26. Chen, J., X.-W. Zhu, and W.-C. Ju, "Design of x-band microstrip cross-coupled bandpass filter," *Acta Microwave Sinica*, Vol. 30, No. 02, 54–57, 2014.
27. Ali, M., et al., "Miniaturized high-performance filters for 5G small-cell applications," *2018 IEEE 68th Electronic Components and Technology Conference (ECTC)*, 1068–1075, 2018.
28. Duan, K., P. Zhang, D. Cheng, Y. Song, L. Huang, and M. Li, "Design of new miniaturized broadband bandpass filter based on SIR," *2019 Photonics & Electromagnetics Research Symposium — Fall (PIERS — Fall)*, 1640–1644, Xiamen, China, Dec. 17–20, 2019.
29. Xu, H. and W. Sheng, "The X-band microstrip filter design," *2017 7th IEEE International Symposium on Microwave, Antenna, Propagation, and EMC Technologies (MAPE)*, 351–355, 2017.
30. Wang, G., C. Chen, and J. Li, "A compact wideband bandpass filter based on stepped impedance line sections," *2018 IEEE International Conference on Consumer Electronics-Taiwan (ICCE-TW)*, 1–2, 2018.